SPECIAL SECTION: ORIGINAL ARTICLE

Satellite altimeter observations of nonlinear Rossby eddy–Kuroshio interaction at the Luzon Strait

Quanan Zheng · Chang-Kuo Tai · Jianyu Hu · Hongyang Lin · Rong-Hua Zhang · Feng-Chun Su · Xiaofeng Yang

Abstract Satellite altimeter sea level data from 1993 to 2008 are used to analyze the interaction of nonlinear Rossby eddies with the Kuroshio at the Luzon Strait (LS). The sea level anomaly data show that the west Pacific (WP) is a source of nonlinear Rossby eddies, and the South China Sea (SCS) is a sink. The LS serves as a gateway between the two. The scale analysis indicates that eddies with a radius larger than 150 km are strong enough to significantly alter the Kuroshio and are able to modify the local circulation pattern. Statistical analysis indicates that the probability for eddies to penetrate through the Kuroshio may reach at least 60%. A case study of an anticyclonic mesoscale eddy passing through the LS in June–July 2004 indicates that the Kuroshio behaves as an unsteady flow with its stream path frequently modified, in a way of cutting off, meandering and branching during its interaction with the eddy. We therefore suggest that nonlinear Rossby eddies may play a significant role in modification of the local circulation system near the LS and in exchanges of the mass, momentum and energy between the WP and the SCS.

Q. Zheng (✉)
Department of Atmospheric and Oceanic Science,
University of Maryland, College Park, MD 20742, USA
e-mail: quanan@atmos.umd.edu

C.-K. Tai
National Oceanic and Atmospheric Administration,
National Environmental Satellite, Data, and Information Service,
5200 Auth Road, Camp Springs, MD 20746, USA

J. Hu · H. Lin
State Key Laboratory of Marine Environmental Science,
College of Oceanography and Environmental Science,
Xiamen University, Xiamen 361005, Fujian, China

R.-H. Zhang
Earth System Science Interdisciplinary Center,
University of Maryland, College Park, MD 20740, USA

F.-C. Su
Department of Marine Biotechnology and Resources,
National Sun Yat-sen University, Kaohsiung 80424, Taiwan

X. Yang
Institute of Remote Sensing Applications,
Chinese Academy of Sciences, Beijing, China

1 Introduction

The western boundary of the northern Pacific comprises the Japan Islands, the East China Sea continental slope, the Taiwan Island, and the Philippines Islands. The Luzon Strait between the Taiwan Island and the Luzon Island is a large gap in the Pacific western boundary. The LS occupies a quite broad water area from 18.5 to 22.0°N and from 120 to 122°E. The topographic map in Fig. 1 shows that the strait connects the South China Sea (SCS) deep basin on the west side, with an average depth of 3,000 m, and the west Pacific (WP) deep basin on the east side with an average depth of 5,000 m. Within the strait, there are two generally parallel, north–south oriented, submarine ridges sandwiching a deep trench of more than 4,000 m. Recent cruise measurements and numerical studies reveal that the LS is a key passage for the SCS Throughflow, which connects the tropical Pacific to the Indian Ocean, and has an important influence on the circulation in the Indonesian

Fig. 1 A bottom topographic map of the LS and its adjacent area
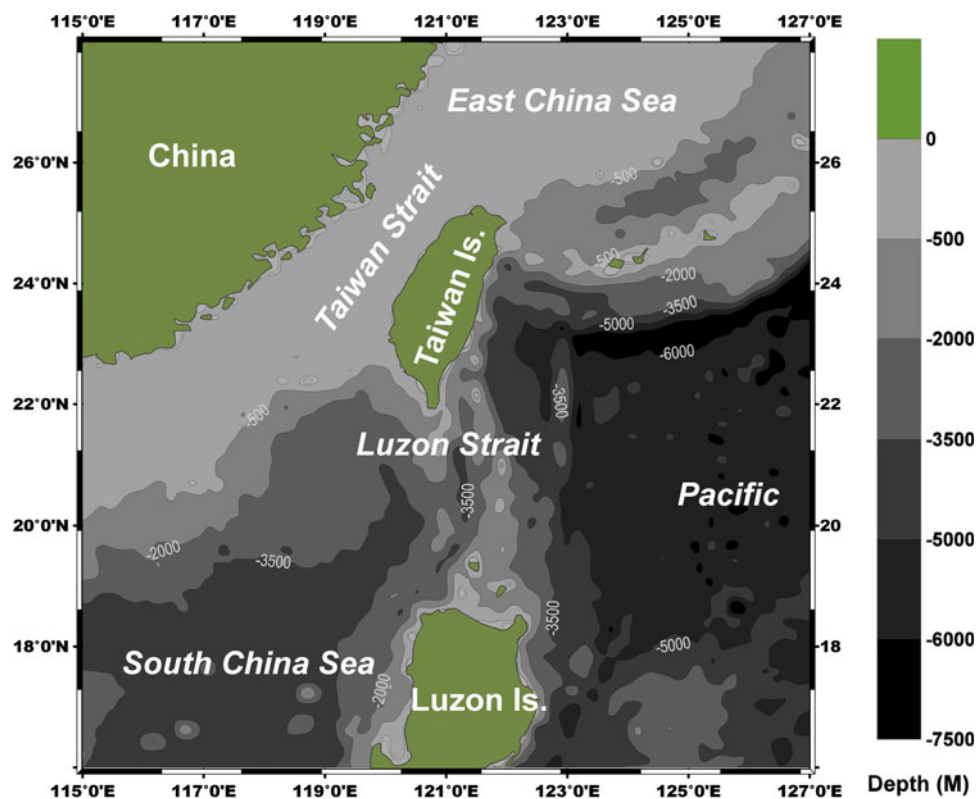
Seas (Fang et al. 2005; Qu et al. 2005, 2006; Tozuka et al. 2007; Yu et al. 2007).

The Kuroshio, a western boundary current in the WP, evolves from the North Equatorial Current in the offshore area east of the Philippines between 16 and 18°N latitude. The current flows generally northward along the east coast of Luzon Island (LS), the east coast of Taiwan Island, and the Okinawa Trough in the East China Sea, and then returns back to the WP through the Tokara Strait (Hu et al. 2008). Along this path, the LS is an opening in a solid wall. Thus, attention should be paid to the behavior of the Kuroshio. Previous investigators have observed the oceanic processes from sub-mesoscale to large scale in the LS, such as the Kuroshio intrusion into the SCS through the LS (Farris and Wimbush 1996; Ho et al. 2004; Hu et al. 2008; Li and Wu 1989; Nitani 1972; Xue et al. 2001; Yuan et al. 2006), eddy shedding from the Kuroshio (Jia and Liu 2004; Li et al. 1998), the Rossby waves propagating into the SCS through the LS (Hu et al. 2001), sub-mesoscale vortex train in the strait (Zheng et al. 2008a), and internal wave generation sources (Zheng et al. 2008b).

Some previous investigators have used satellite altimeter data for studies of mesoscale dynamics in the LS and SCS since the early 1990s (Ho et al. 2000a, b; Hu et al. 2001; Li et al. 2002, 2004, 2007; Shaw et al. 1999; Wang et al. 2000a, 2003). Using satellite altimeter sea surface height data, they have also revealed that in the subtropical Pacific

there is a zonal band between 20 and 25°N, in which mesoscale wave-like eddy trains with a wavelength of 800–1,000 km propagate westward all year round. Their average phase speed is of $O(0.1 \text{ m s}^{-1})$ (Chelton and Schlax 1996; Ho et al. 2009; Hu et al. 2001).

The LS is centered at around 20°N. This position just faces eastward to the zonal band of mesoscale eddy trains as shown in satellite altimeter sea level maps. Its north–south width is approximately 400 km, and the average depth is around 2,000 m. The position and the sufficient dimensions provide favorable conditions for mesoscale eddies to pass through the strait and enter the SCS. Hu et al. (2001) pointed out that the Rossby waves propagate into the SCS through the LS. While Li et al. (2004) recognized the waves in the SCS may be triggered by eddies of the WP interacting with the Kuroshio or other reasons (such as Kuroshio instability), but it is not the same wave that propagates directly into the SCS. Recently, Sheu et al. (2010) examined the dynamic conditions when eddies can or cannot freely propagate through the Kuroshio and the LS into the SCS using numerical modeling and satellite altimeter data analysis methods.

Obviously, for the problem of mesoscale eddy propagation into the SCS, there are two important questions, which still need to be further clarified. The first question is what role the Kuroshio plays in coupling between the SCS and the WP. The second question is what role the LS plays in this process.

This study aims to answer the above two questions by the analysis of 16 years satellite altimeter sea level data from 1993 to 2008. Section 2 gives a scale analysis for comparison of total momentum and total kinetic energy of the Kuroshio segment to that of eddies. Section 3 describes the satellite data used in this study. Section 4 contains statistical analysis of the dataset. Section 5 interprets a Maps of Absolute Dynamic Topography (MADT) time series in June–July 2004, which contains detailed information of an anticyclonic eddy penetrating the Kuroshio and the LS and entering the SCS, as well as the Kuroshio branching forced by multiple eddies. Sections 6 and 7 include discussion and conclusions.

2 Scale analysis

2.1 Scales of dynamic parameters

We use the scale analysis method to estimate what will happen if the Kuroshio collides or interacts with an eddy. For the Kuroshio, the horizontal width of its main path is about 100 km (Li et al. 2000; Yuan et al. 2006), i.e., $L_k = O(100$ km$)$. Observations indicate that the Kuroshio depth varies seasonally from 600 m in winter (Yuan et al. 2000a) to 1,400 m in summer (Yuan et al. 2000b), thus $D_k = O(1000$ m$)$ should be a reasonable estimate for the depth scale of the Kuroshio. The typical speed value of the Kuroshio surface current is $O(1$ m s$^{-1})$ (Li et al. 2000; Yuan et al. 2006), but the speed decreases with the depth. Thus $O(0.5$ m s$^{-1})$ should be a reasonable scale for the depth-averaged current speed of the Kuroshio, v_k.

For mesoscale eddies in the WP, the diameters vary within a range from 200 to 400 km, thus $L_e = O(300$ km$)$ should be a reasonable estimate for the horizontal length scale of eddies. The observations and modeling results indicate that the depths of eddies are deeper than 1,000 m (Li et al. 2000; Wang et al. 2000b), thus $D = O(1,000$ m$)$ should be a reasonable estimate for the vertical scale of eddies. From time series analysis of sea level anomaly (SLA) data (see Sect. 4.1), we determine that the scale of horizontal propagation speed of eddies, u_e, is $O(0.1$ m s$^{-1})$, and the scale of angular speed of eddies, ω, is $O(5 \times 10^{-6}$ s$^{-1})$ on the basis of the data listed in Table 1.

2.2 Ratios of total momentum and total kinetic energy of Kuroshio to eddy

For the Kuroshio, the total momentum carried by a segment of the same length scale as the mesoscale eddy L_e ($=2R$; here R is the eddy radius) can be written as

$$M_k = \rho \cdot \text{Volume} \cdot v_k = 2\rho R L_k D_k v_k, \tag{1}$$

where ρ is the water density, and other scale parameters as defined above.

For the eddy, the total momentum is a vector sum of two components: the horizontal motion momentum and the rotation momentum, thus the total momentum amplitude is

$$
\begin{aligned}
M_e &= \sqrt{M_{\text{horizontal}}^2 + M_{\text{rotation}}^2} \\
&= \sqrt{(\rho \cdot \text{Volume} \cdot u_e)^2 + \left(2\pi\rho D\omega \int_0^R r^2 \, dr\right)^2} \\
&= \pi\rho R D \left(u_e^2 + \frac{4}{9}\omega^2 R^4\right)^{1/2},
\end{aligned}
\tag{2}
$$

where the angular speed ω is assumed as a constant (solid body assumption). From Eqs. 1 and 2, we obtain the total momentum ratio of Kuroshio to eddy

$$\Gamma_1 = \frac{M_k}{M_e} \approx \frac{3}{2\pi} \frac{v_k L_k}{\omega R^2}. \tag{3}$$

Similarly, for the Kuroshio, the total kinetic energy can be written as

$$E_k = \frac{1}{2}\rho \cdot \text{Volume} \cdot v_k^2 = \rho R L_k D_k v_k^2. \tag{4}$$
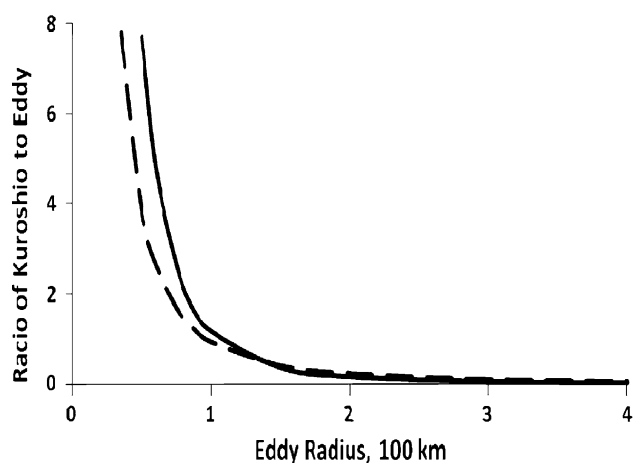
For the eddy, the total kinetic energy is

$$
\begin{aligned}
E_e &= E_{\text{horizontal}} + E_{\text{rotation}} \\
&= \frac{1}{2}\rho \cdot \text{Volume} \cdot u_e^2 + \pi\rho D\omega^2 \int_0^R r^3 \, dr \\
&= \frac{\pi}{4}\rho R^2 D(2u_e^2 + \omega^2 R^2).
\end{aligned}
\tag{5}
$$

From Eqs. 4 and 5, we obtain the total kinetic energy ratio of Kuroshio to eddy

$$\Gamma_2 = \frac{E_k}{E_e} = \frac{4}{\pi}\left(\frac{L_k}{R}\right)\left(\frac{D_k}{D}\right)\left(\frac{v_k^2}{2u_e^2 + \omega^2 R^2}\right). \tag{6}$$

The graphic expressions of Eqs. 3 and 6 are shown in Fig. 2. One can see that the curves of total momentum and total kinetic energy ratios of Kuroshio to eddy monotonically decrease with the eddy radius. From the view of the momentum, Γ_1 is greater than 1 for the eddy radius $R < 100$ km, implying that, for eddies with radii smaller than 100 km, the Kuroshio will play a dominant role when they collide or interact with each other. For $R > 100$ km, Γ_1 decreases quickly with the increase in R. For $R > 200$ km, Γ_1 is smaller than 0.5, implying that the eddy will play a dominant role when they collide or interact with each other.

From the view of the kinetic energy, Γ_2 is greater than 1 for the eddy radius $R < 150$ km, implying that for eddies with radii smaller than 150 km, the Kuroshio will play a

Fig. 2 Ratios of total momentum (*dashed line*) and total kinetic energy (*solid line*) of the Kuroshio segment to the eddy versus the eddy radius

dominant role when they collide or interact with each other. For $R > 150$ km, Γ_2 decreases quickly with the increase in R. For $R > 200$ km, Γ_2 is smaller than 0.5, implying that the eddy will play a dominant role when they collide or interact with each other, if the potential energy is supposed to be a small quantity or in balance between the Kuroshio and the eddy.

In the case to be examined in Sect. 5, the eddy that collided with the Kuroshio east of LS from June 26 to July 3, 2004 (eddy Ew in Fig. 5a, b, below) has a radius greater than 200 km. Substituting this value into Eqs. 3 and 6 shows that the total momentum and the total kinetic energy of the eddy is 4.2 and 6.4 times that of the Kuroshio, respectively. Thus, we may predict that the Kuroshio cannot keep its path unchanged under the forcing of this big eddy. In other words, the Kuroshio has no longer served as a dynamic shield for the LS and the SCS.

3 Satellite altimeter sea level data

This study uses two kinds of satellite altimeter sea level datasets. Both datasets are merged products derived from TOPEX/POSEIDON (T/P), Jason-1/2 (French–US altimeter satellites), ERS-1/2 (European Remote Sensing satellites), and ENVISAT (European Remote Sensing satellite) altimeters. The products are distributed by Archiving Validation and Interpretation of Satellite Data in Oceanography (AVISO), the Centre National d'Etudes Spatiales of France.

The first datasets are Maps of Sea Level Anomalies (MSLA) and geostrophic velocity anomalies from 1993 to 2008. The datasets contain multi-mission gridded sea surface heights computed with respect to a 7-year mean. The

maps are Cartesian gridded with a spatial resolution of 1°/3 by 1°/3. The temporal interval is 7 days.

The second datasets are MADT from 1993 to 2008. The datasets contain along-track sea surface heights above geoid, thus dynamic topography is the sum of SLA and mean dynamic topography. The maps are Cartesian gridded with a spatial resolution of 1°/4 by 1°/4. The temporal interval is 3–4 days. The products used in the following case study are obtained through National Oceanic and Atmospheric Administration (NOAA) Pacific Marine Environmental Laboratory (PMEL).

Dynamically, the rotation motion of mesoscale eddies is controlled by the sea level height gradient between the eddy center and the surrounding water (Pedlosky 1987). Thus on a sea level dynamic height map, an eddy should appear as a circle-like or elliptical pattern with closed and densely distributed sea level contour lines. Chow et al. (2008) and Hu (2008) compared such SLA patterns with simultaneous Argos drifter trajectories in the SCS. They found that the Argos drifter trajectory appears as a vortex-like pattern when passing through an elliptical SLA pattern. This implies that the elliptical SLA patterns represent a rotating water mass, i.e., an eddy. On the other hand, we should also consider limitations of the data products. For the state-of-the-art satellite altimeter, the sea level height measurement accuracy is around 4 cm. The spatial resolution of two satellite altimeter products used in this study is better than 1°/3. Thus in order to avoid misinterpretation, we add three more thresholds to distinguish a mesoscale eddy: (1) the absolute value of sea level height difference of the eddy center from the mean sea level must be greater than 7.5 cm, (2) the eddy radius must be greater than 50 km, and (3) the water depth is greater than 1000 m.

An example of the MSLA is shown in Fig. 3. One can see that anti-cyclonic (high SLA in red) eddies and cyclonic (low SLA in blue) eddies to the east of LS show up clearly. Examples of the MADT are shown in Fig. 5a–f (below). One can see that the MADT data contain not only the details of eddies but also the mean flow information.

4 Statistical analysis of satellite altimeter sea level data

4.1 Time series analysis of SLA feature propagation

Satellite altimeter sea level data show that the mesoscale eddy trains as shown in Fig. 3 originate from the central Pacific. They are generated by the nonlinear growth, like wave breaking, of large-scale Rossby waves (Zheng et al. 1994), and carried by the waves. Thus, they are called non-linear Rossby eddies. The time series analysis of SLA feature propagation reveals the following two important points: (1) the large-scale waves in the Pacific propagate westward

Fig. 3 An example of MSLA in the LS and its adjacent waters on July 19, 1995. Anticyclonic eddies appear as elliptic high SLA patterns (*red*) and cyclonic eddies as elliptic low SLA patterns (*blue*). *Arrows* represent the geotropic velocity vectors (by courtesy of AVISO)
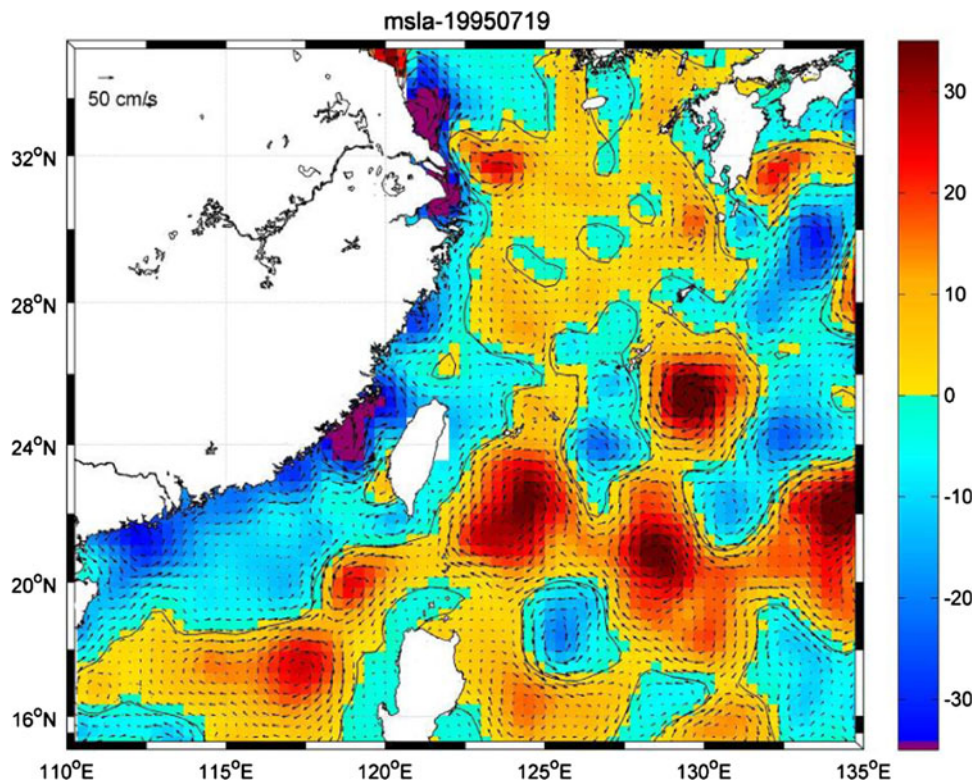
all the way to the SCS, and (2) from Hu et al. (2001), we obtain a reasonable estimate for the scale of horizontal propagation speed of observed eddy trains to be $O(0.1 \text{ m s}^{-1})$.

4.2 Statistics of eddy distribution near the LS

The propagation track of a nonlinear Rossby eddy is controlled by the large-scale Rossby waves and also modified by the local circulation. When they approach the western boundary and meet the strong western boundary current and the boundary topography, their tracks would be modified. Thus, we may find useful information on the interactions of eddies with the Kuroshio and the boundary topography through examining the spatial distribution and trajectories of eddies. Figure 4 shows the distribution of eddy centers and trajectories near the LS from 18° to 23°N and from 116° to 126°E observed from 16 years of MSLA. One can see that there are two high distribution density areas of eddy centers and trajectories located on the west and east sides of LS, respectively. Inbetween the two, there is a low density area inside the LS. In the central LS between 20° and 21°N, there is a zonal channel connecting the two high density areas. Some trajectories on the WP side show northward or northwestward propagations, implying the Kuroshio modification to the eddy tracks.

From yearly distribution of eddies in the WP (122–126°E), the LS (120–122°E), and the SCS (116–120°E), we count the total numbers (cyclonic and anticyclonic) of observed eddies as 241 (124, 117) in the WP, 72 (44, 28) in the LS, and 193 (105, 88) in the SCS, respectively (Lin et al. 2010). Note that the temporal resolution of MSLA products is 7 days. Thus, eddies lasting for longer than 7 days may be observed twice or more, and eddies lasting for shorter than 7 days may be missing. Therefore, the numbers of observed eddies may only be used to estimate the probability of eddies being observed under the sampling rate of satellite altimeters (once per 7 days). If we take the probability of eddies being observed per unit area (5° latitude by 1° longitude) in the WP as 1, then it is 0.6 in the LS and 0.8 in the SCS.

For eddies occurring in the LS, the local dynamic conditions define that the probability for local generation is ignorable. The probability for the SCS origin is also ignorable, because only one case was observed during the period of 16 years. Thus, we suppose that they basically originate from the WP. Using the probabilities of eddies being observed in the WP and the LS, we estimate that penetration probability of eddies through the Kuroshio may reach at least 60%.

5 A case study of an eddy passing through the LS

5.1 Time series data interpretation

Figure 5a–f shows an MADT time series of the study area from June 26 to July 14, 2004. One can see a complete
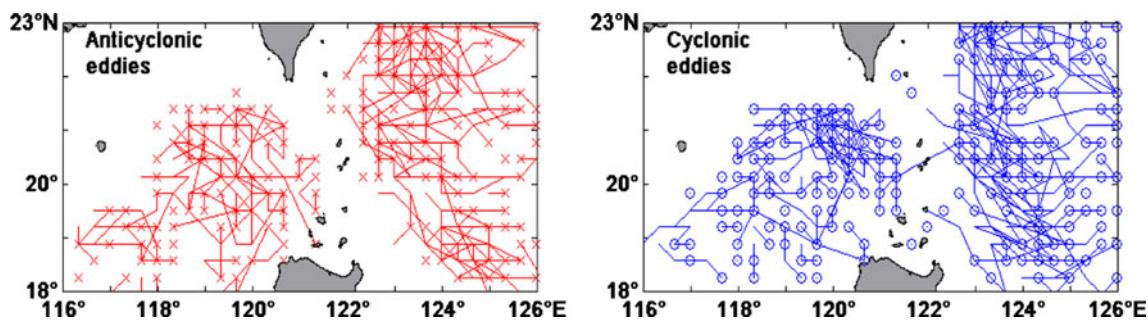
Fig. 4 Distribution of eddy centers and trajectories near the LS derived from MSLA from 1993 to 2008

process of an anticyclonic mesoscale eddy penetrating through the Kuroshio and the LS into the SCS.

On image of June 26, 2004 shown in Fig. 5a, one can see a double-core high sea level area with color codes from light green to light brown occupying a water area east of the LS between 20–24°N and 122–125°E. This imagery represents an anticyclonic (warm) eddy as marked by Ew. Examining the patterns of Ew, one can find that an important feature on its middle western side, i.e., a westward protrusion (marked as Pw) centered at 21.5°N, 122°E. It is this westward protrusion that finally evolved into a mesoscale eddy penetrating the LS. On the other hand, the appearance of this westward protrusion seems to be associated with the pressure of a westward propagating cyclonic eddy (marked as Ec) to Ew, which was centered at 22.5°N, 125°E, immediately behind Ew. In the meantime, the Kuroshio (marked as arrows) formed a westward meander toward the LS.

On June 30, 2004 (Fig. 5b), eddy Ec had further moved about a ¼° westward across 124°E since June 26. Double-core anticyclonic eddy Ew had decomposed. Its north core had become a warm jet extending north-northeastward. The westward protrusion of Ew had grown to a warm tongue with a south–north width of about 100 km. The warm tongue carried an eddy-like core Ed as marked by a dashed circle. The westward Kuroshio meander had also grown, and its front had entered the LS.

On July 3, 2004 (Fig. 5c), the westward extending warm tongue of Ew had separated from Ew and evolved to an independent warm eddy (marked as Ed), which was centered at 21°N, 120°E in the deep basin of SCS west of the LS. The horizontal size of eddy Ed reached 150 km (south–north) by 200 km (west–east), and the dynamic height difference of its center from the surrounding waters reached 20 cm, referred to the absolute dynamic height of 230 cm (hereafter). These facts imply that the eddy had grown up to be a strong anticyclonic one. In the meantime, the northward Kuroshio mean path was cut off by a cyclonic eddy of 150 km by 200 km centered at 19°N,

123.5°E (marked as Ec2). The dynamic height difference of its center from the surrounding waters reached −30 cm, implying that eddy Ec2 was a strong one. From following Fig. 5d and e, one can see that Ec2 originated from the WP and propagated westward with an average speed of 0.15 m s^{-1}. The Kuroshio north of eddy Ec2 along 20°N became a zonal current and branched into two at 20°N, 122°E: one northward-flowing branch, and another westward-flowing branch. The westward-flowing branch like a jet injected into the LS and SCS first, and then looped back to the Pacific. These features are consistent with that of traditionally defined Kuroshio Loop Current (KLC) (Farris and Wimbush 1996; Li and Wu 1989; Shaw et al. 1996; Xue et al. 2001). Eddy Ed was located at frontal end of the jet and had a high sea level belt (235 cm) still linked with the parent eddy Ew, implying that Ed was evolved from Pw and flowed westward with the KLC.

On July 7, 2004 (Fig. 5d), the general imagery patterns of absolute dynamical topography were similar to that of July 3, but eddy Ed was getting weaker and the KLC further intruded northwestward. The KLC front had reached 21.6°N, 117°E and a new eddy centered at 22°N, 118°E was generated. Meanwhile, another westward extending warm tongue with a size of 200 km by 200 km grew out of big warm eddy Ew. Its front had reached the LS center. The dynamical height difference of the center of cold eddy Ec2 from the surrounding waters reached −40 cm, implying that it was further strengthened.

On July 10, 2004 (Fig. 5e), the general imagery patterns of absolute dynamic topography were similar to that of July 7, but KLC intruded further northwestward. Its front had reached 21°N, 115.3°E and the new eddy originally centered at 22°N, 118°E had grown up and moved southwestward to 21.7°N, 117.7°E. Warm eddy Ed was further weakened, and disappeared on the image of July 14 (Fig. 5f). The front of the warm tongue of Ew had passed the central line of LS.
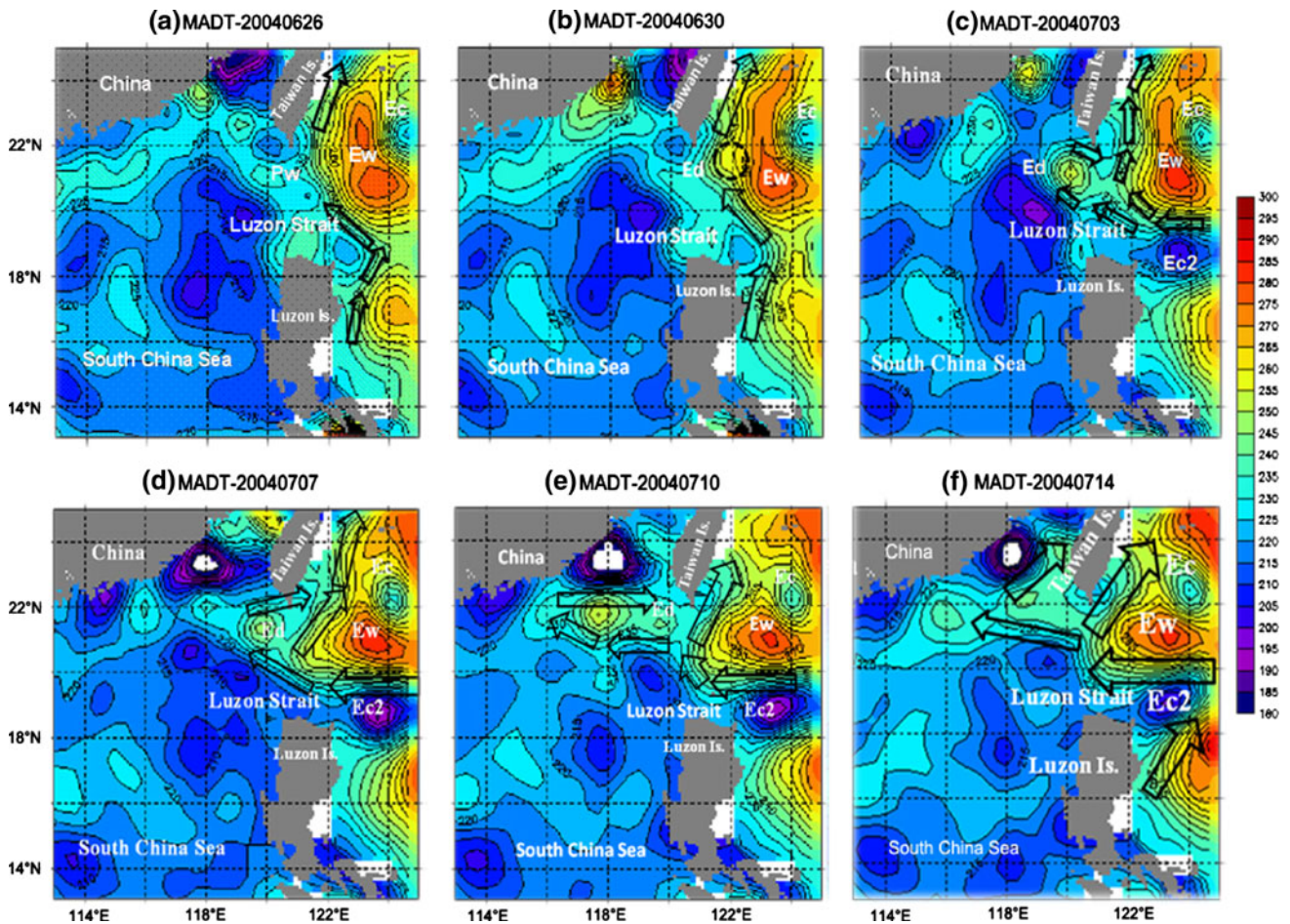
Fig. 5 A map of absolute dynamical topography of the study area (by courtesy of NOAA PMEL). **a** June 26, **b** June 30, **c** July 3, **d** July 7, **e** July 10 and **f** July 14, 2004

5.2 Dynamic parameter calculation and analysis

The dynamic parameters of mesoscale eddy Ed measured or calculated from Fig. 5a are listed in Table 1. The parameters are calculated in a cylindrical coordinate system (not shown). The origin is set at the eddy center, the z axis is positive up, the radius axis is positive away from z axis, and the azimuth axis is positive anti-clockwise perpendicular to the radius axis, respectively.

The quasi-geostrophic momentum equation is used to calculate the azimuthally velocity

$$V_\theta = -\frac{g}{f}\frac{\partial \eta}{\partial r}, \tag{7}$$

where g is the gravitational acceleration, f is the Colioris parameter, η is the sea surface dynamic height, and r is the radius distance. The angular velocity ω is calculated as

$$\omega = \frac{V_\theta}{R}, \tag{8}$$

where R is a radius of the eddy or a radius of the local curvature for KLC, which is defined as

$$R = \frac{\partial s}{\partial \alpha}, \tag{9}$$

where s is the length of an arc, and α is a corresponding angle of the arc. In the cylindrical coordinate system, the vorticity is defined as

$$\begin{aligned}
\vec{\varsigma} &= \nabla \times \vec{V} \\
&= \left(\frac{1}{r}\frac{\partial V_z}{\partial \theta} - \frac{\partial V_\theta}{\partial z}\right)\vec{r}_0 + \left(\frac{\partial V_r}{\partial z} - \frac{\partial V_z}{\partial r}\right)\vec{\theta}_0 \\
&\quad + \left(\frac{1}{r}\frac{\partial(rV_\theta)}{\partial r} - \frac{1}{r}\frac{\partial V_r}{\partial \theta}\right)\vec{k}_0,
\end{aligned} \tag{10}$$

where V_r, V_θ and V_z are the velocity components projected on the three coordinate axis, respectively, $\vec{r}_0$, $\vec{\theta}_0$ and $\vec{k}_0$ are unit vectors, respectively. If the azimuthal velocity is a dominant component, i.e., V_r and V_z are negligible, Eq. 10 has an approximate form

$$\vec{\varsigma} = \left(-\frac{\partial V_\theta}{\partial z}\right)\vec{r}_0 + \left(\frac{1}{r}\frac{\partial(rV_\theta)}{\partial r}\right)\vec{k}_0. \tag{11}$$

In our case, the first term of Eq. 11 is assumed to be much smaller than the second term, and the rotation is

Table 1 Dynamic parameters of eddy Ed and KLC derived from the MADT time series from June 26 to July 14, 2004

	Time				
	June 30	July 3	July 7	July 10	July 14
Location	WP	WP-SCS	SCS	SCS	SCS
Eddy Ed					
Propagating speed[a] (cm s^{-1})	−9.9	−67	−71	−8.2	
Radius[b] (km)	60	70	70	60	0.0
Azimuthally velocity[a] (cm s^{-1})	−16	−58	−40	−26	0.0
Angular velocity[a] ($\times 10^{-6}$ s^{-1})	−2.7	−7.8	−6.0	−4.4	0.0
Vortices[a] ($\times 10^{-6}$ s^{-1})	−5.4	−16	−12	−8.9	0.0
Kuroshio Loop Current					
Radius of curvature[b] (km)		152	121	93	
Azimuthally velocity[a] (cm s^{-1})		−69	−50	−31	0.0
Angular velocity[a] ($\times 10^{-6}$ s^{-1})		−4.6	−4.1	−3.3	0.0
Vorticity[a] ($\times 10^{-6}$ s^{-1})		−9.9	−8.2	−6.6	0.0

[a] Relative accuracy (est.) better than 20%

[b] Measurement accuracy 13 km

assumed to be uniform, thus the vorticity has an approximate form

$$\varsigma = 2\omega. \tag{12}$$

From Table 1, one can see that the westward propagation speed of Ed is 0.099 m s^{-1} in the WP east of the LS, and decreases to 0.071 and 0.082 m s^{-1} in the SCS west of the LS. These results are consistent with previous results (Hu et al. 2001). An important finding here is that the average westward propagation speed of Ed between June 30 and July 3, 2004 reached as high as 0.67 m s^{-1}, which is nearly one order higher than that in the WP and the SCS. This speed is almost the same as the average velocity of KLC as listed in Table 1, implying that the eddy passed the LS with the jet-like KLC, when it was branched from the Kuroshio main path.

In summary, the findings of the case study are summarized as follows:

1. The case shows a complete process of a nonlinear Rossby eddy penetrating the Kuroshio and the LS and propagating into the SCS. A big anticyclonic eddy with a size of 500 km by 300 km, located at the immediate east of LS, initiated the process. A westward propagating cyclonic eddy just behind the big anticyclonic eddy further pressed the big anticyclonic eddy to form a westward protrusion or a warm tongue. Meanwhile, the Kuroshio is forced to form a westward meander toward the LS.

2. The eddy penetrating through the LS and entering into the SCS occurred simultaneously with the Kuroshio branching. Their westward propagation speed reached as high as 0.67 m s^{-1}. The conditions for branching occurrence are: (1) the strong anticyclonic eddy east of the LS (central dynamic height

45–50 cm higher than the local mean) forces the Kuroshio meander to develop to a westward warm water tongue; and (2) the strong cyclonic mesoscale eddy (central dynamic height 30–40 cm lower than the mean) northeast of the Luzon Island cutoff the north–south path of Kuroshio and forces it to become a zonal current along 20°N directly pointing to the LS.

3. The westward branch of the Kuroshio intrudes into the LS and the SCS and forms KLC in the northeast SCS deep basin. The appearance of eddy Ed in the SCS demonstrates that nonlinear Rossby eddies propagate into the SCS not only in a way of wave motion but also carrying the mass. Eddy Ed originated from a big eddy in the WP, but it has not been the original eddy. Its size has been modified by the Kuroshio and the LS.

6 Discussion

6.1 On Kuroshio branching

The phenomenon of Kuroshio water intrusion into the SCS has been reported by the previous investigators since the 1970s (Caruso et al. 2006; Centurioni and Niiler 2004; Ho et al. 2004; Nitani 1972). But the mechanism for the intrusion remains unclear. Some investigators attributed it to the winter northeasterly monsoon winds, and concluded that the intrusion would occur in winter only (Farris and Wimbush 1996; Wang and Chern 1987). Some investigators attributed it to eddy shedding, so that it might occur at any season (Jia and Liu 2004; Metzger and Hurlburt 2001). Yuan et al. (2006) suggested that the Kuroshio water intrudes into

the SCS in all seasons, implying that the monsoon winds are not a major mechanism responsible for such intrusions. The previous investigators also found that there are two modes for the intrusion path: a direct intrusion and a loop current. The latter is defined as an anticyclonic circulation passing through the LS twice, in-flowing into the SCS first and out-flowing back to the WP later (Li and Wu 1989). The two intrusion modes are only used to describe the patterns of Kuroshio intrusion path in the SCS. Tracing back to their upstream sources, however, the detailed dynamics, i.e. under what dynamic conditions the Kuroshio branches an intrusion current from its mainstream, remains unclear.

In Sect. 5, a case of Kuroshio branching process in July 2004 has been examined (see Fig. 5c–f). An interpretation sketch is shown in Fig. 6. The dynamic conditions for Kuroshio branching are summarized as follows. A strong cyclonic mesoscale eddy with a scale of $O(200$ km) northeast of Luzon Island, marked as Ec2 in Fig. 5c–f, cuts the Kuroshio mainstream path off. This cyclonic eddy and a strong anticyclonic eddy, with a scale of $O(400$ km) east of the LS marked as Ew in Fig. 5b–f, sandwich the Kuroshio and force it become a zonal current flowing toward the LS. At the west outlet of narrow channel formed by the two eddies, the zonal current becomes a jet-like flow with divergent stream lines. Thus the fluid vorticity represented by the radial stream line varies due to varying curvature radii of the lines. The fluid of large negative vorticity combines with the anticyclonic eddy and forms a north branch, while the fluid of large positive vorticity combines with the cyclonic eddy. In principle, it should form a south branch. However, it fails to develop due to the physical blockage of Luzon Island and the dynamic blockage of anticyclonic Warm Eddy 2. The rest portion of fluid keeps flow westward and forms a west branch. Thus the Kuroshio splits into two branches, the north branch flows northward along the Kuroshio mainstream path, and the west branch flows westward entering the SCS through the LS. A critical vorticity for the fluid turning northward can be estimated from Fig. 5c–f. For example, a minimum value of critical vorticity calculated from Fig. 5c is $O(5 \times 10^{-6}$ s^{-1}).

Therefore, this case shows that the essential mechanism of Kuroshio branching is the mesoscale eddy forcing or the interaction between the Kuroshio and mesoscale eddies originating from the tropical Pacific. Their vertical scale is the same as that of the Kuroshio, and the horizontal scale is much larger than the local width of the Kuroshio. Thus, they are capable of modifying the Kuroshio and even cutting off its path. On the other hand, this situation indicates that the Kuroshio should not be treated as a steady current in the area east
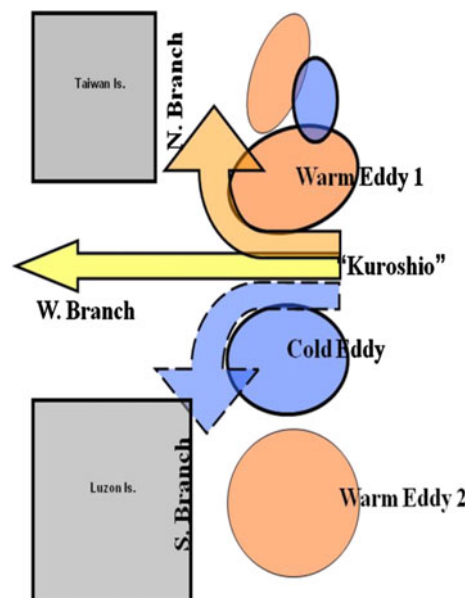
Fig. 6 An interpretation sketch illustrating the dynamic conditions for Kuroshio branching observed in July 2004. Warm and cold eddies mean anti-cyclonic and cyclonic eddies, respectively

of LS. This is true not only in summer but also in other seasons as shown as satellite-tracked drifter data (Hu et al. 2008).

6.2 On eddy penetration through the Kuroshio

The case study in Sect. 5 reveals that the eddy Ed passed through the LS at a speed of 0.67 m s^{-1} together with the Kuroshio branching. This also further reveals the mechanism of how does an eddy "penetrate" the Kuroshio. It does not look like a bullet penetrating through a wall at all. The eddy has never propagated in or penetrated through the Kuroshio current field. Instead, the eddy cuts off the Kuroshio path, forces it to branch into the LS, and enters the SCS together with the Kuroshio branch. The entire process looks more like a wall that is suddenly pushed and crashes down. Obviously, this sudden change process is an unsteady and highly nonlinear process.

6.3 On formation of a low SLA belt in the LS

Statistics of eddy distribution near the LS in Sect. 4.2 indicate that the probability of eddies being observed in the LS is lower than that in the WP and the SCS. Moreover, the panels of temporal–spatial distribution of sea level fluctuation across the LS shows a low value belt along the north–south central line of the strait (Hu et al. 2001; Li et al. 2007). Hu et al. (2001) pointed out that the Rossby waves sometimes propagate into the SCS through the LS,

implying that the low SLA belt is independent of the Rossby wave propagation.

Here, we use two mechanisms to explain the phenomenon. The first is sampling probability. The data and analysis results in Sects. 4 and 5 reveal that it is no problem for mesoscale eddies to propagate from the WP into the SCS through the LS, and the Kuroshio is unable to play a role of dynamic shield there all the time. We believe that the satellite altimeter sea level values are dependent upon the statistical occurrence probability of dynamic processes like mesoscale eddies. Observed at a fixed point, like the LS, the statistical occurrence probability of an eddy should be reversely proportional to the speed of the eddy passing through the strait and the orbit re-visit period of the satellite altimeter. As listed in Table 1, the average propagation velocities of mesoscale eddies in the WP and the SCS are -0.099 m s^{-1} and -0.071 to -0.082 m s^{-1}, respectively. The velocity reaches as high as -0.67 m s^{-1} when the eddy passes through the LS. This implies that the statistical probability for random observation to "catch" the eddy occurrence in the LS is only 11% of the probability in the SCS and 15% of that in the WP. The temporal resolution of SLA data or orbit re-visit period of satellite altimeters available is about 3–7 days. Thus, the statistical probability for the satellite altimeters to "catch" eddies in the LS must be much less than that in the SCS and the WP. This results in the time-averaged SLA values in the LS lower than that in the SCS and the WP. The second reason is eddy decay due to side friction. In the WP, the depth is $O(5,000$ m$)$, and horizontal scales are $O(>5,000$ km$)$, while in the LS the depth is shoaling to $O(2,000$ m$)$ and the horizontal scales become $O(400$ km by 200 km$)$. Thus, both the horizontal viscosity and the vertical viscosity in the LS are larger than that in the WP and the rotation motion of eddies will be decayed when they enter the LS from the WP. At the same time, the SLA of eddies will naturally decrease and the average SLA values in the LS will be lower than that in the WP. When eddies enter into the SCS, they may gain vorticity from the KLC or local circulation. The rotation motion of eddies may be strengthened again, so that the SLA values are also higher than that in the LS.

6.4 On influence of submarine ridges in the LS on eddy propagation

In the LS, there are two generally parallel, north–south oriented, submarine ridges with a depth of about 2,500 m. In this study, we estimate that the depth scales of the Kuroshio and mesoscale eddies are $O(1,000$ m$)$. Thus, we did not consider the influence of submarine ridges on the processes of interest.

7 Conclusions

In this study, we have quantified the role of nonlinear Rossby eddies played in coupling between the SCS and the WP with emphasis on their interaction with the Kuroshio and the LS. Our conclusions are based on the analysis of satellite altimeter sea level data products, MSLA and MADT, from 1993 to 2008. With the scale analysis, statistical analysis and a case study, we have reached the following conclusions.

7.1 A fundamental understanding

Nonlinear Rossby eddy trains, consisting of the cyclonic and anticyclonic mesoscale eddies and originating from the tropical Pacific, propagate westward, and end in the SCS all year round. Thus, the tropical Pacific is a source and the SCS is a sink of the mesoscale eddies. The LS serves as a gateway between the two.

The results of scale analysis and case study indicate that ratios of the total momentum and the total kinetic energy of Kuroshio segment to that of an eddy with the same horizontal length scale sharply decrease with the eddy radius. For small eddies with radii smaller than 100 km, the ratios are greater than 1, and the Kuroshio would play a dominant role when they collide or interact with each other. For large eddies with radii greater than 150 km, the ratios are smaller than 0.5, and eddies would play a dominant role when they collide or interact with the Kuroshio.

7.2 The role of Kuroshio

Before entering the LS, eddies meet the Kuroshio first. For small eddies, the Kuroshio might serve as a dynamic shield to block eddies' westward propagation. For large eddies, the Kuroshio is unable to keep itself unchanged under the forcing by a large eddy or multiple eddies. In contrast, the Kuroshio mainstream path is modified by eddies, including cutting off, meandering and branching.

The case study in Sect. 5 gives a complete description of Kuroshio branching process. The eddy penetrates through the LS and enters into the SCS simultaneously with the Kuroshio branch, which then forms the KLC in the northeast SCS and the LS.

7.3 The role of LS

The LS provides a channel for westward propagating nonlinear Rossby eddies and the Kuroshio branch to enter the SCS. Its north and south side boundaries as well as shallower bottom topography constrain the stream lines to be converged in the LS and form a dynamic orifice.

Effects of the dynamic orifice to eddy are threefold. First, the propagation speed of an eddy would be accelerated. Second, the rotation speed of the eddy would be decelerated due to the friction of side and bottom boundaries. Third, the eddy size would be shrunk. Thus, the LS plays a role most like a high-pass dynamic filter for nonlinear Rossby eddy trains. Relatively small size eddies would pass through the LS with the Kuroshio branch and finally enter the SCS.

References

Caruso M, Gawarkiewicz GG, Beardsley R (2006) Interannual variability of the Kuroshio Current intrusion in the South China Sea. J Oceanogr 62(4):559–575

Centurioni LR, Niiler PP (2004) Observations of inflow of Philippine Sea surface water into the South China Sea through the Luzon Strait. J Phys Oceanogr 34(1):113–121

Chelton DB, Schlax MG (1996) Global observation of oceanic Rossby waves. Science 272(5259):234–238

Chow C-H, Hu J-H, Centurioni LR, Niiler PP (2008) Mesoscale Dongsha cyclonic eddy in the Northern South China Sea by drifter and satellite observations. J Geophys Res 113:C04018. doi:10.1029/2007JC004542

Fang G, Susanto D, Soesilo I, Zheng Q, Qiao F, Wei Z (2005) A note on the South China Sea shallow interocean circulation. Adv Atmos Sci 22(6):945–954

Farris A, Wimbush M (1996) Wind-induced Kuroshio intrusion into the South China Sea. J Oceanogr 52(6):771–784

Ho C-R, Kuo N-J, Zheng Q, Soong YS (2000a) Dynamically active areas in the South China Sea detected from TOPEX/POSEIDON satellite altimeter data. Rem Sens Environ 71(3):320–328

Ho C-R, Zheng Q, Soong YS, Kuo N-J, Hu J-H (2000b) Seasonal variability of sea surface height in the South China Sea observed with TOPEX/POSEIDON altimeter data. J Geophys Res 105(C6):13981–13990

Ho C-R, Zheng Q, Kuo N-J, Tsai C-H, Huang NE (2004) Observation of the Kuroshio Intrusion region in the South China Sea from AVHRR data. Intl J Rem Sens 25(21):4583–4591

Ho C-R, Zheng Q, Zheng Z-W, Kuo N-J, Tai C-K, Su F-C (2009) Reply to comment by A. Wada et al. on "The importance of pre-existing oceanic conditions to upper ocean response induced by Super Typhoon Hai-Tang". Geophys Res Lett 36:L09604. doi:10.1029/2009GL037443

Hu J-H (2008) Eddies with Kuroshio intrusion to the Northern South China Sea. In: Liu AK et al (eds) Satellite remote sensing of South China Sea. Tingmao, Taipei, Taiwan, pp 171–185

Hu J, Kawamura H, Hong H, Kobashi F, Wang D (2001) 3–6 months variation of sea surface height in the South China Sea and its adjacent ocean. J Oceanogr 57(1):69–78

Hu X, Xiong X, Qiao F, Guo B, Lin X (2008) Surface current field and seasonal variability in the Kuroshio and adjacent regions derived from satellite-tracked drifter data. Acta Oceanol Sin 27(3):11–29

Jia Y, Liu Q (2004) Eddy shedding from the Kuroshio bend at Luzon Strait. J Oceanogr 60(6):1063–1069

Li L, Wu B (1989) The Kuroshio loop current in the South China Sea? On circulation of the northeastern South China Sea. J Oceanogr Taiwan Strait 8(1):89–95

Li L, Nowlin WD, Su J (1998) Anticyclonic rings from the Kuroshio in the South China Sea. Deep Sea Res I 45(9):1469–1482

Li L, Wu R, Guo X (2000) Seasonal circulation in the South China Sea—a TOPEX/POSEIDON satellite altimetry study. Acta Oceanol Sin 22(6):13–26

Li L, Jing C, Zhu D (2007) Coupling and propagating of mesoscale sea level variability between the western Pacific and the South China Sea. Chin Sci Bull 52(12):1699–1707

Li Y, Li L, Lin M (2002) Mesoscale eddies in southwestern Taiwan derived from TOPEX/Poseidon. Acta Oceanol Sin 24(Suppl 1):163–170

Li Y, Li L, Jing C, Cai W (2004) Characteristics of tempo-spatial sea level height variability in northeast South China Sea. Chin Sci Bull 49(5):702–709

Lin H, Hu J, Zheng Q (2010) Statistics and analysis of mesoscale eddies in the South China Sea and the western Pacific based on 16-year altimeter data. Acta Oceanol Sin (submitted)

Metzger EJ, Hurlburt HE (2001) The nondeterministic nature of Kuroshio penetration and eddy shedding in the South China Sea. J Phys Oceanogr 31(7):1712–1732

Nitani H (1972) Beginning of the Kuroshio. In: Stommel H, Yashida K (eds) Kuroshio: physical aspects of the Japan current. University of Washington Press, Seattle, pp 129–163

Pedlosky J (1987) Geophysical fluid dynamics, 2nd edn. Springer, New York, pp 86–216

Qu T, Du Y, Meyers G, Ishida A, Wang D (2005) Connecting the tropical Pacific with Indian Ocean through South China Sea. Geophys Res Lett 32:L24609. doi:10.1029/2005GL024698

Qu T, Girton G, Whitehead J (2006) Deepwater overflow through Luzon Strait. J Geophys Res 111:C01002. doi:10.1029/2005JC003139

Shaw P-T, Chao S-Y, Liu K-K, Pai S-C, Liu C-T (1996) Winter upwelling off Luzon in the northern South China Sea. J Geophys Res 101(C7):16435–16448

Shaw P-T, Chao S-Y, Fu L-L (1999) Sea surface height variation in the South China Sea from satellite altimetry. Oceanol Acta 22(1):1–17

Sheu W-J, Wu C-R, Oey L-Y (2010) Blocking and westward passage of eddies in the Luzon Strait. Deep Sea Res II (in press)

Tozuka T, Qu T, Yamagata T (2007) Effect of South China Sea throughflow on the Makassar Strait throughflow. Geophys Res Lett 34:L12612. doi:10.1029/2007GL030420

Wang J, Chern C-S (1987) The warm-core eddy in the northern South China Sea. II. A simple mechanism for the establishment and development of the warm-core eddy. Acta Oceanogr Taiwan 18:104–113

Wang L, Koblinsky C, Howden S (2000a) Mesoscale variability in the South China Sea from the Topex/Poseidon altimetry data. Deep Sea Res I 47(4):681–708

Wang H, Yuan Y, Su J, Liu Y (2000b) Three-dimensional numerical calculations of the currents east of Taiwan Island in December 1997. Oceanogr China 12:68–79

Wang G, Su J, Chu P (2003) Mesoscale eddies in the South China Sea observed with altimeter data. Geophys Res Lett 30:L2121. doi:10.1029/2003GL018532

Xue H, Chai F, Shi M (2001) Kuroshio intruded loop current and circulation in the northeastern South China Sea. Oceanogr China 13:23–37

Yu Z, Shen S, McCreary JP, Yaremchuk M, Furue R (2007) South China Sea Throughflow as evidenced by satellite images and numerical experiments. Geophys Res Lett 34:L01601. doi:10.1029/2006GL028103

Yuan Y, Liu Y, Su J, Kaneko A (2000a) The Kuroshio east of Taiwan Island and in the East China sea in the winter of 1997. Oceanogr China 12:11–20

Yuan Y, Liu Y, Su J, Kaneko A, Jiang S (2000b) The Kuroshio east of Taiwan Island and in the East China sea in the summer of 1997. Oceanogr China 12:1–9

Yuan D, Han W, Hu D (2006) Surface Kuroshio path in the Luzon Strait area derived from satellite remote sensing data. J Geophys Res 111:C11007. doi:10.1029/2005JC003412

Zheng Q, Yan X-H, Ho C-R, Tai C-K (1994) The effects of shear flow on propagation of Rossby waves in the equatorial oceans. J Phys Oceanogr 24(7):1680–1686

Zheng Q, Lin H, Meng J, Hu X, Song YT, Zhang Y, Li C (2008a) Sub-mesoscale ocean vortex trains in the Luzon Strait. J Geophys Res 113:C04032. doi:10.1029/2007JC004362

Zheng Q, Song YT, Lin H, Wang D, Hu X, Meng J (2008b) On generation sources of internal waves in the Luzon Strait. Acta Oceanogr Sin 27(3):38–50